Using Ergosterol To Mitigate the Deleterious Effects of Ethanol on Bilayer Structure

Allison N. Dickey, Wen-Sau Yim, and Roland Faller*

Department of Chemical Engineering and Materials Science University of California Davis, Davis, California 95616

Received: April 9, 2008; Revised Manuscript Received: October 30, 2008

In wine fermentations, yeast is exposed to concentrated ethanol solutions. Ergosterol, a sterol that is found in lower eukaryotic membranes, helps preserve the structural integrity of yeast membranes in stressful environmental conditions. A premature arrest in ethanol production due to unknown metabolic changes in yeasts results in undesirably large concentrations of residual sugar and may be caused by the formation of an ethanol-induced interdigitated phase. We use atomistic molecular dynamics simulations to examine the induction of the interdigitated phase in model yeast membranes that contain either 0, 10, 20, 25 mol % ergosterol in ethanol concentrations of 0, 10, 15 vol %. The 25 mol % ergosterol system shows a similar level of interdigitation for the 0 and 10 vol % ethanol solutions, indicating that ergosterol molecules in this system are able to effectively counteract the disruptive behavior of ethanol molecules. However, at a 15 vol % ethanol solution, the amount of interdigitation triples and this ethanol concentration is similar to the concentrations found in stuck fermentations. The other three ergosterol concentrations studied (0, 10, 20 mol %) show larger quantities of interdigitation in the 10 vol % ethanol solution than the 0 vol % solution. Thus, the 25 mol % ergosterol bilayer, which is representative of the ergosterol concentrations seen in yeast membranes, is unique in the systems examined in its ability to delay the onset of ethanol-induced interdigitation. The concentration of ergosterol affects the permeability of a fluid-phase bilayer, where the 10 mol % ergosterol bilayer is more permeable to ethanol than either a bilayer containing no ergosterol molecules or a bilayer containing 20/25 mol % ergosterol. This lipid permeability appears to be correlated with the existence of a lipid region whose lipids neither have direct contact with ergosterol molecules nor exhibit bulk lipid/lipid interactions.

Introduction

Ethanol is a renewable fuel that can be produced from a variety of biomass sources. For example, corn is the most common ethanol feedstock in the United States, sugar cane is often used in Brazil because it results in low fermentation costs, and straw is used in the European Union.[1] To convert these crops into ethanol, yeast cells ferment the starch-derived glucose in biorefineries. A large percentage of ethanol produced in the United States comes from corn and the production of corn-derived ethanol has increased from an average of 6500 barrels a day in 1980 to an average of 417 000 barrels a day in 2007. This increase in ethanol production could be considerably larger if plants that contain cellulose, such as prairie grass and switch grass, and biomass such as corn stover, were used as an additional feedstock. However, converting cellulose cheaply to fermentable sugars is challenging because expensive pretreatment is required to release and degrade cellulose.[2]

In wine production, yeast (*Saccharomyces cerevisiae*) is used to convert sugar from grapes into ethanol and fermentation conditions are optimized to obtain high ethanol yields. Wine fermentations typically have ethanol concentrations ∼12−14 vol % ethanol, although some strains of *S. cerevisiae* can survive ethanol concentrations of up to 19 vol %.[3] Fermentations generally take 7−10 days to reach completion; however, sluggish fermentations take longer and stuck fermentations leave high concentrations of residual sugar in the final product.[4] Stuck fermentations are undesirable because wines containing a high sugar content are vulnerable to microbial spoilage.[4] The sugar to ethanol conversion is reduced under stressful fermentation conditions, such as nutrient limitation, low pH, lack of oxygen, temperature extremes, and the presence of toxic substances. Incomplete fermentations that have a high residual sugar content have been correlated with a loss of plasma membrane transport protein activity.[4] How these transport proteins enter the latent state is mechanistically not understood.

Ergosterol is the sterol component found in the plasma membranes of lower eukaryotes such as yeast.[5] Ergosterol is similar to cholesterol, with the only structural differences being that ergosterol has two additional double bonds (7 and 22 in Figure 1) and a methyl group (24 in Figure 1). It was proposed that double bond 22 (Figure 1) increases lipid alkyl chain stabilization and makes the membranes more resistant to ethanol permeation than membranes that contain cholesterol.[6] Because the fluidity of a membrane is important for maintaining the conformational state of transmembrane proteins, specifically transport proteins in this case, it is important to understand how ethanol molecules in a fermentation broth will affect membrane structure. The composition of a yeast membrane is dynamic and is dependent upon environmental conditions. For example, it has been found that the presence of ethanol molecules results in the production and inclusion of unsaturated fatty acids and ergosterol in the membrane.[3,4] In comparing two strains of *S. cerevisiae*, Chi et al. found that the less-ethanol-tolerant strain increased its ergosterol/phospolipid ratio in response to ethanol, whereas the more-ethanol-tolerant strain did not. This showed that the less-tolerant strain attempted to counteract the fluidizing effect of ethanol by increasing its ergosterol concentration.[7]

One deleterious effect of ethanol is that it induces the formation of the interdigitated phase in lipid membranes.[8−11] This phase is characterized by the intertwining of lipid molecules

* Corresponding author. E-mail: rfaller@ucdavis.edu.

10.1021/jp803092z CCC: $40.75
Published on Web 02/04/2009

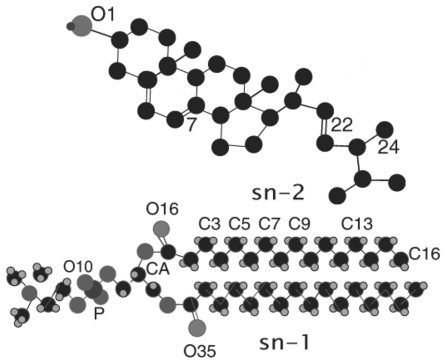

Figure 1. Attached to the DPPC phosphorus atom (P) is oxygen atom O10. Carbon atom CA is in the DPPC glycerol group, oxygen atom O16 is in the *sn*-2 carbonyl group and oxygen atom O35 is in the *sn*-1 carbonyl group. The *sn*-1 carbonyl atoms are closer to the bilayer center than the *sn*-2 carbonyl atoms. The oxygen atom in the ergosterol hydroxyl group is labeled O1 and the two double bonds and methyl groups that differentiate ergosterol from cholesterol are labeled 7, 22, and 24.

from opposing bilayer leaflets and because interdigitation results in a change in the physical structure of a bilayer, it will also likely alter the conformation of neighboring transport proteins. In a micropipette aspiration (MPA) experiment, Tierney et al. examined how the structure of vesicles composed of dipalmitoylphosphatidylcholine (DPPC) lipids and ergosterol changes with ethanol concentration.[12] The vesicles contained ~10−25 mol % ergosterol, where it has been found that *S. cerevisiae* from an anaerobic chemostat fermentation has 21−26 mol % ergosterol and *Trypanosoma cruzi*, a protozoan human parasite, has 23 mol % ergosterol.[13,14] Stuck fermentations have residual sugar concentrations that are larger than 4 g/L and will typically occur between 12 and 16 vol % ethanol.[3,4,12,15] Using MPA techniques, Tierney et al. found interdigitation in this ethanol concentration range, reinforcing the link between an ethanol-induced interdigitated phase and stuck fermentations.[12]

In a single-component bilayer, if the system temperature is below the lipid phase transition point (T_m), the lipids will exist in a solid-ordered (S_o) gel state. If the system temperature is above the T_m, the lipids will exist in a fluidized liquid-disordered (L_d) state. However, for multicomponent bilayers, the transition between the S_o and the L_d phases is complex and may contain multiple transition points.[16,17] A bilayer containing sterols is often associated with the L_o phase, which is a phase not found in single-component bilayers. The lipids in this phase characteristically have a diffusivity that is similar to L_d phase lipids and a hydrocarbon chain order that is similar to S_o phase lipids. Both the DPPC/cholesterol and DPPC/ergosterol phase diagrams have been experimentally determined and the formation of L_o domains in a DPPC/ergosterol bilayer requires a larger sterol concentration than the formation of L_o domains in a DPPC/cholesterol bilayer.[16,17]

Tierney et al. found that vesicles containing 20−25 mol % ergosterol can withstand a larger concentration (an additional 7 vol %) of ethanol than pure DPPC vesicles before the onset of interdigitation.[12] In this study, we use atomistic molecular dynamics simulations to examine how ergosterol molecules mitigate the fluidizing effect that ethanol has on cellular membranes. Because the composition of a yeast membrane can depend on the genus, strain, and environmental conditions, it is difficult to capture all membrane components in a model system.[3] Yeast membranes often contain phosphoglycerolipids that have one saturated chain and one monounsaturated acyl chain, such as 1-palmitoyl-2-oleoyl-sn-glycero-phosphocholine (POPC).[18] Because ethanol-induced interdigitation has been examined extensively in experiments using bilayers composed of DPPC, we also use DPPC in this study.[9,10,12,19] We examine a DPPC bilayer at two temperatures, $T = 298$ K and $T = 325$ K, where the T_m for DPPC is 314 K.[20] During wine fermentations, the broth temperature should not exceed 303 K and hence only the simulations at $T = 298$ K are directly relevant to fermentations.[4] Also, it has been found experimentally that ethanol molecules induce the interdigitated phase at temperatures below that of the lipid T_m.[8] Thus, interdigitation that is observed at $T = 325$ K does not mimic the experimentally reported interdigitated phase because it is not in the correct temperature regime but rather gives an estimate for the range of membrane fluidities that ergosterol can modulate.

Methods

We constructed 18 bilayers that contained DPPC and ergosterol molecules and 6 bilayers that contained only DPPC lipids. For all 24 systems, there was a total of 128 DPPC/ergosterol or DPPC molecules per bilayer, with 64 per leaflet. Four concentrations of ergosterol molecules were examined: 0 mol %, 9.4 mol % (which will be referred to as 10 mol %), 20.3 mol % (which will be referred to as 20 mol %), and 25 mol %. The 10 mol % ergosterol systems have 6 ergosterol molecules per leaflet and the ergosterol:lipid (e:l) ratio is 1:10; the 20 mol % ergosterol has 13 ergosterol molecules per leaflet and an e:l ratio of 1:4; the 25 mol % has 16 molecules per leaflet and an e:l ratio of 1:3. These bilayers were bathed in one of three ethanol solutions: 0 vol %, 10 vol % (120 ethanol molecules), and 15 vol % (200 ethanol molecules). Each system contained 3618 water molecules. The ergosterol and ethanol concentrations used in each system are listed in Table 1 ($T = 298$ K), Table 2 ($T = 325$ K), and Table 3 (bilayers with 0 mol % ergosterol).

The lipid structures for each simulation were based on a united atom model where the lipid acyl chain hydrogen atoms are not explicitly represented. The ergosterol crystal structure came from the protein crystallography database in Uppsal,a[21] and the sterol charges are from a cholesterol study by Hoeltje et al.[22] To construct a DPPC/ergosterol bilayer, one lipid from the end of a 250 ps simulation performed by Tieleman et al. (http://moose.bio.ucalgary.ca) was selected and replicated on a 8 × 8 grid.[23] This lipid lattice represented the top leaflet, and it was copied and rotated 180° around the *y*-axis to create the

TABLE 1: Bilayer Properties at $T = 298$ K[a]

properties	10−0	10−10	10−15	20−0	20−10	20−15	25−0	25−10	25−15
equil time (ns)	145	120	104	380	55	92	97	207	76
A_{DPPC} (nm^2)	0.551			0.489			0.480		
A_{ERG} (nm^2)	0.272			0.249			0.244		
$A_{molecule}$ (nm^2)	0.525	0.649	0.721	0.440	0.523	0.606	0.420	0.461	0.539
thickness (nm)	4.37	3.94	3.44	4.64	4.48	3.95	4.66	4.55	4.49
phase	$S_o/S_o + L_o$			$S_o + L_o$			$S_o + L_o$		

[a] The heading row specifies the system as *x*−*y*, where *x* = ergosterol mol % and *y* = ethanol vol %.

TABLE 2: Bilayer Properties at $T = 325$ K[a]

properties	10−0	10−10	10−15	20−0	20−10	20−15	25−0	25−10	25−15
equil time (ns)	94	85	90	97	102	101	119	96	77
A_{DPPC} (nm^2)	0.623			0.561			0.537		
A_{ERG} (nm^2)	0.293			0.263			0.252		
$A_{molecule}$ (nm^2)	0.580	0.676	0.748	0.482	0.595	0.649	0.455	0.534	0.601
thickness (nm)	3.98	3.80	3.33	4.42	4.00	3.74	4.52	4.36	3.96
phase	L_d			$L_d + L_o$			$L_d + L_o$		

[a] The heading row specifies the system as $x-y$, where x = ergosterol mol % and y = ethanol vol %.

bottom leaflet. DPPC lipids were chosen at random from the top and bottom leaflets and replaced with ergosterol molecules. Once the bilayers contained the appropriate number of ergosterol molecules, 3618 water molecules were added by extending the simulation box in the z direction. Initially, the simulations were run for 20 ps at 350 K with the DPPC phosphorus atoms and all ergosterol atoms restrained. The atoms in the ergosterol molecules that were not found in a ring-structure were then released and the three systems were simulated for an additional 20 ps at 350 K. Next, all ergosterol atom restraints were removed and the temperature was reduced to either 325 or 298 K and simulated for 20 ps. Finally, all remaining restraints (DPPC phosphorus atoms) were removed and the simulations at both $T = 298$ K and $T = 325$ K were equilibrated for 1 ns. The simulation box was extended a second time to add the ethanol molecules for those systems that had 10 vol % and 15 vol % ethanol solutions.

The force field parameters for the lipids were a combination of nonbonded parameters described by Berger et al. and the GROMOS87 force field.[24,25] The GROMOS87 force field parameters were used for the ergosterol molecules and the water parameters are from the Simple Point Charge (SPC) model.[26] The simulations were performed using the MD package GROMACS 3.3.1, and some of the data analysis was performed using GROMACS tools.[27−29] Each system was simulated at two temperatures: 298 and 325 K. The simulations were coupled to a heat bath using a Berendsen thermostat[30] with a coupling time constant of 0.1 ps. The system pressure was maintained anisotropically at 1.0 bar using a Berendsen barostat with a coupling constant of 0.2 ps. Bond lengths were constrained using the LINCS algorithm.[31] The Lennard-Jones interaction cutoff was 1.0 nm with a switch function starting at 0.8 nm. The electrostatics were calculated using the PME method[32] with a short-range cutoff of 1.0 nm. The time step was 2 fs. The equilibration times are shown in Tables 1, 2, and 3. The simulations were deemed equilibrated when the area per lipid had stabilized. The measurement of area per lipid is frequently used to monitor simulation equilibration as it is an experimentally accessible property and it reflects the state of a membrane. The equilibration phase was followed by an additional 10 ns of simulations used for data analysis. The center of mass motion of each leaflet was removed at every time step.

In analyzing the partitioning of ethanol molecules into the bilayer, we have assigned the ethanol molecules to one of five bins on the basis of their distance from the nearest ergosterol molecule. We divided the 10 ns trajectories into four 2 ns segments (1−3, 3−5, 5−7, and 7−9 ns) and used the configuration from the middle of each 2 ns segment ($t = 2$, 4, 6, and 8 ns) to calculate the ergosterol/ethanol distances and make final bin assignments based on the average of the four segments. In this way, the ethanol molecules located in each bin were updated every 2 ns. The area per bin was calculated using this method as well and the final area was averaged over the top and bottom leaflets.

Results

System Dimensions. We calculated the area per DPPC lipid and ergosterol molecule for non-ethanol containing systems using equations for multicomponent bilayers

$$A_{DPPC} = \frac{2A(x)}{(1 - x)N_{LIPID}}\left[1 - \frac{xN_{LIPID}V_{ERG}}{V(x) - V_{WATER}N_{WATER}}\right] \quad (1)$$

$$A_{ERG} = \frac{2A(x)V_{ERG}}{V(x) - V_{WATER}N_{WATER}} \quad (2)$$

that were developed by Hofsäss et al.[33] $A(x)$ is the xy area of the simulation cell, A_{DPPC} is the area per lipid, A_{ERG} is the area per ergosterol, N_{LIPID} is the combined number of lipid and ergosterol molecules, N_{ERG} is the number of ergosterol molecules, N_{WATER} is the number of water molecules, $V(x)$ is the volume of the simulation cell, V_{ERG} is the volume of a single ergosterol molecule, x is N_{ERG}/N_{DPPC} and V_{WATER} is the volume of a water molecule. $V_{WATER} = 0.0312$ nm^3 and assuming that the volume of a cholesterol and ergosterol molecule are similar, $V_{ERG} = 0.593$ nm^3, which is the volume of a cholesterol molecule.[33,34]

The naming scheme for the systems used in this paper is ergosterol concentration (mol %) − ethanol concentration (vol %)$_{temp}$. The area per molecule, which is calculated by dividing the x and y dimensions of the simulation cell by the number of lipids per leaflet, was calculated for all systems and are shown in Tables 1 and 2. Hsueh et. al generated a partial phase diagram for DPPC/ergosterol bilayers for a temperature range of 300−326 K, and we use their diagram to identify the phases for the non-ethanol containing systems.[17] Because our membranes contain only 128 DPPC and ergosterol molecules, it is quite possible that the bilayers do not exist in the phases that are seen experimentally for a given composition and temperature. However, because the conditions that result in a phase change in a complex lipid mixture and the structural dimensions of raft domains are still under investigation, we use the experimentally reported phase diagrams as a guide for estimating the lipid phases in the simulations. Table 3 shows the results for those systems that do not contain ergosterol molecules and the phases of the systems without ethanol are based on the DPPC T_m.[20] The phases of the systems that contain 120 ethanol molecules are based on the DPPC/ethanol phase diagrams generated by Ohki et al.[8]

For gel phase DPPC at $T = 292$ K, it was found using X-ray diffraction that the A_{DPPC} is 0.472 ± 0.005 nm^2. This value is much smaller than the simulated value of 0.621 nm^2 that we found for $T = 298$ K (Table 3). This difference may indicate that the $T = 298$ K (gel phase) simulations have not yet reached equilibrium. In a simulation study of DPPC lipids in the gel

TABLE 3: Bilayer Properties for Non-ergosterol Systems

properties	$0-0_{298}$	$0-0_{325}$	$0-10_{298}$	$0-10_{325}$	$0-15_{298}$	$0-15_{325}$
equil time (ns)	101	129	58	62	62	58
$A_{molecule}$ (nm^2)	0.621	0.665	0.722	0.756	0.780	0.816
thickness (nm)	**3.81**	3.73	3.52	3.49	3.42	3.33
phase	gel	liquid	interdigitated	liquid		

and liquid phases, Leekumjorn et al. calculated the DPPC hysteresis curves from heating and cooling scans where the temperature ranged from 250 to 350 K.[35] In the cooling scan, the A_{DPPC} was ~0.63 nm^2 at 300 K and in the heating scan, the A_{DPPC} was ~0.58 nm^2 at 300 K. From the heating curves, a DPPC T_m between 300 and 310 K could be observed. However, from the cooling curves, a clear phase transition was not observable and the A_{DPPC} changed at a slower rate than in the heating curves.[35] For our bilayers that did not contain ergosterol molecules, the initial system configurations came from the end of a 250 ps simulation performed by Tieleman et al. at T = 325 K.[23] Even though we did not use a simulated annealing technique as was done by Leekumjorn et al., the simulations still dropped from a temperature of 325 K to a temperature of 298 K. Hence, these simulations in a sense follow the cooling curve scans produced by Leekumjorn et al. and the similarities in A_{DPPC} (0.621 nm^2 at T = 298 K vs ~0.63 nm^2 at T = 300 K) are visible.[35] Because the A_{DPPC} at T = 298 K is higher than the experimental value, the simulated bilayer thickness value (3.8 nm) will be smaller than the experimental bilayer thickness (4.5 nm).[36] The simulated bilayer thickness at T = 325 K (3.73 nm), however, is similar to the results from an X-ray diffraction experiment, which found the liquid phase DPPC bilayer thickness to be 3.96 nm.[37]

Using NPT simulations, Cournia et al. examined a DPPC bilayer that contained 40 mol % ergosterol and they found an A_{DPPC} = 0.471 ± 0.002 nm^2 at 309 K and 0.479 ± 0.002 nm^2 at 323 K.[38] These values are slightly smaller than A_{DPPC} = 0.480 nm^2 at 298 K and 0.537 nm^2 at 323 K that are shown in Table 1 and Table 2 for the 25 mol % ergosterol systems. However, as the ergosterol concentrations increase, the A_{DPPC}, A_{ERG}, and $A_{Molecule}$ values decrease and, therefore, the differences between the two sets of A_{DPPC} values may be the result of differing ergosterol concentrations. The bilayer thickness is related to the area per lipid and is defined as the distance between the phosphorus atom density profile peaks in the two leaflets. In the tables, we see that bilayer thicknesses increase with increasing ergosterol concentration and decrease with increasing ethanol concentration.

The A_{ERG} for the systems that do not contain ethanol molecules have average values of 0.255 nm^2 at 298 K and 0.269 nm^2 at 325 K. These values are somewhat smaller than the crystalline cholesterol area (37 Å^2) and similarly small areas for cholesterol relative to the crystalline area have been seen in other simulation studies, with the disparity being attributed to differences in the crystalline and the bilayer environments.[33,39,40] The A_{ERG} values at T = 325 K can be compared with a simulation study that examined DPPC/cholesterol bilayers at T = 323 K, where the cholesterol concentrations ranged from 0 to 40 mol %.[33] The area per cholesterol at 10 mol % cholesterol was 0.289 nm^2 (A_{DPPC} = 0.582 nm^2) and the area per cholesterol at 25 mol % cholesterol was 0.276 nm^2 (A_{DPPC} = 0.554 nm^2).[33] The A_{ERG} at 10 mol % is 0.293 nm^2 (A_{DPPC} = 0.623 nm^2) and the A_{ERG} at 25 mol % ergosterol is 0.252 nm^2 (A_{DPPC} = 0.537 nm^2). The 0.024 nm^2 difference seen at 25 mol % sterol may be due to the structural variances between the ergosterol and cholesterol molecules. Tierney et al. found that DPPC/ergosterol bilayers in the L_o phase are less condensed than their DPPC/cholesterol counterparts.[12]

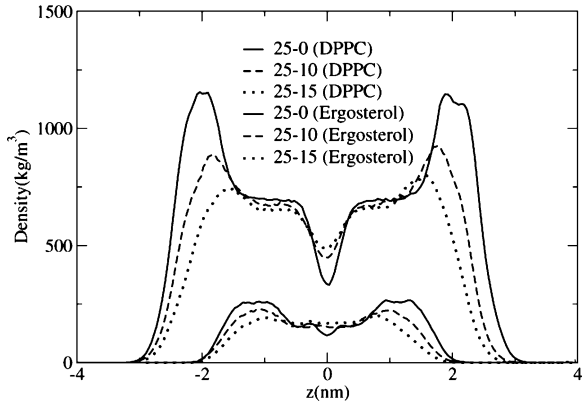

Figure 2. Density profiles for DPPC and ergosterol systems 25−0, 25−10, and 25−15 at T = 325 K.

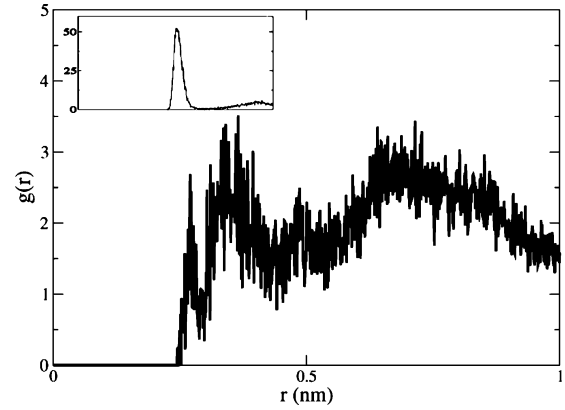

Figure 3. RDF between ergosterol atom O1 and DPPC atom O10 and O16 for system $10-0_{325}$. The prominent RDF is for DPPC atom O10 and the figure inset is the RDF for DPPC atom O16.

Density Profiles. Figure 2 shows the density profiles for the 25−0, 25−10, and 25−15 systems at T = 325 K. The figure shows that, as the ethanol concentration is increased, the prominent DPPC headgroup peaks shift closer together and have reduced peak densities. Similarly, the ergosterol density profiles show broadened peaks in the presence of ethanol. Figure 3 is a radial distribution function (RDF) for system $10-0_{325}$ between the ergosterol hydroxyl oxygen atom (O1) and a DPPC phosphodiester oxygen atom (O10). The figure inset displays the RDF between ergosterol atom O1 and a DPPC *sn*-2 carbonyl oxygen atom (O16). In comparing the two RDF profiles, we find that it is 12.5 times more likely that atom O1 will be located 0.25 nm from atom O16 than from atom O10. The favorable interaction between the DPPC carbonyl oxygen atoms and the ergosterol hydroxyl group has been seen in other DPPC/sterol experiments and simulations.[38,40−42] Even though Figure 3 only shows data for one simulation, the preference that atom O1 shows for atom O16 is seen in all systems. The RDF between ergosterol atom O1 and the DPPC *sn*-1 carbonyl oxygen atom (O35) is not as large as that of O16 and the O1/O35 RDF is only 3 times larger than the RDF between atom O1 and atom O10. The ethanol molecule hydroxyl groups also show a preference for the *sn*-2 DPPC O16 atoms compared to the DPPC O10 atoms (Figure 4). As was seen with the ergosterol molecules, the RDF peak between the ethanol hydroxyl groups and the *sn*-1 DPPC O35 atoms is smaller than the ethanol/O16 peak, but larger than the ethanol/O10 peak. The favorability of the *sn*-2 DPPC carbonyl groups as hydrogen bond acceptors

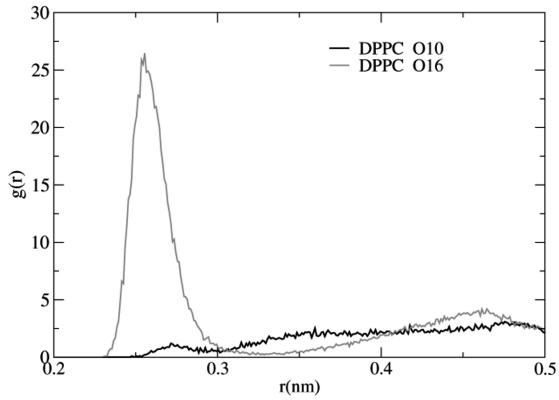

Figure 4. RDF between the ethanol hydroxyl oxygen atom and DPPC atom O10 and O16 for system $10-0_{325}$.

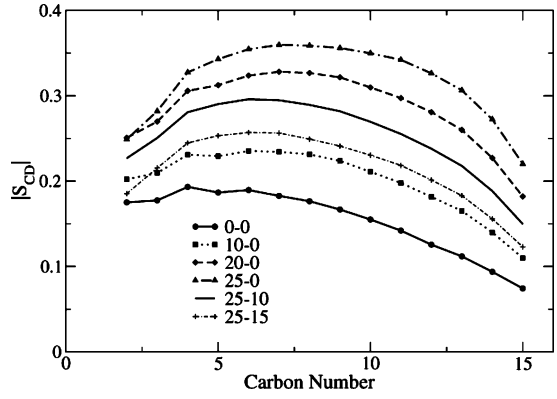

Figure 5. DPPC *sn*-2 acyl chain order parameters for $T = 298$ K.

for both ergosterol and ethanol may cause the ergosterol density peak broadening that occurs with increasing ethanol concentrations in Figure 3. As the number of ethanol molecules in the bilayer is increased, the competition between the ergosterol and ethanol molecules for an interaction site at a DPPC carbonyl group will increase. Thus, it may be more favorable for the ergosterol molecules to shift toward the bilayer center than crowd the ethanol molecules at the carbonyls. In comparing the O1/O35 RDF between the 0, 10, and 15 vol % ethanol systems at $T = 325$ K, the systems that contained 10 and 15 vol % ethanol had increased peak intensities when compared with the 0 vol % ethanol systems for all ergosterol concentrations. A corresponding decrease in the O1/O16 RDF peak intensity was seen for these systems. At $T = 298$ K, all ergosterol concentrations showed an increased O1/O35 peak at 15 vol % ethanol compared to the 0 vol % systems. However, the 20 and 25 mol % ergosterol systems did not show increased O1/O35 rdf peak intensities at 10 vol % ethanol. This indicates that for 20 and 25 mol % ergosterol, the vicinity around the DPPC O16 atoms becomes saturated at ~10−15 vol % ethanol, where the extra kinetic energy at $T = 325$ K promotes the shifting of ergosterol toward the bilayer center at lower ethanol concentrations than at $T = 298$ K.

Chain Order. In the L_o phase, the lipid chain order is similar to the chain order seen in the S_o phase and the lateral lipid fluidity is similar to that of the L_d phase.[43] The order parameter is a useful measurement in simulations because it can be compared with the experimental deuterium order parameter, which can be determined through nuclear magnetic resonance spectroscopy measurements. Because the hydrocarbon chain structures are based on the united atom model, hydrogen atoms are not explicitly represented and the C−H bonds are reconstructed assuming tetrahedral geometry of the CH_2 groups. The order parameter is defined as

$$S_{CD} = \frac{1}{2}\langle 3\cos^2\theta_{CD} - 1\rangle \quad (3)$$

where θ_{CD} is the angle between the CD bond and the bilayer normal in experiments and in simulations the CD bond is replaced by the CH bond. The order parameters are defined for carbon atoms C_{n-1} through C_{n+1} and thus for DPPC, order parameters are calculated for atoms C_2 through C_{15}.

In a recent study of POPC/ergosterol bilayers, Hsueh et al. found that the lipid acyl chain order increases with an increase in ergosterol concentration. However, the order of the POPC acyl chains is only dependent on ergosterol concentrations up to 25 mol %.[18] In comparison, it has been found that DPPC lipid chain order can be increased by the inclusion of up to 42 mol % ergosterol.[17] It has been seen in both simulations and experiments that ethanol molecules cause a reduction in the acyl chain order parameters in lipid bilayers.[19,44,45] Similarly, we found that the acyl chain order parameters decrease with increasing ethanol concentration and increase with increasing ergosterol concentration. Figure 5 shows the order parameters for $T = 298$ K and similar results are seen for systems at $T = 325$ K (not shown).

To determine if ergosterol can counteract this fluidizing effect of ethanol, we calculated the relative difference in *sn*-2 acyl chain S_{CD} values (X) between the ergosterol (S_{CD}^{erg})/nonergosterol (S_{CD}) containing bilayers using

$$X = \frac{S_{CD}^{erg} - S_{CD}}{S_{CD}} \quad (4)$$

This method of calculating the relative increase/decrease in chain order was presented by Barry et al. in a ^{2}H NMR study of the effects of ethanol molecules on dimyristoylphosphatidylcholine (DMPC)/cholesterol bilayers.[19] Figure 6a shows that in the presence of a 0 vol % ethanol solution, X is very similar for systems at $T = 298$ K and $T = 325$ K.

However, panels b and c of Figure 6 show that as the ethanol concentration is increased, the systems at $T = 298$ K have a greater increase in order than the systems at $T = 325$ K. As we saw in Tables 1 and 2, the bilayers at $T = 325$ K become more fluidized and have a larger area per molecule in the presence of ethanol than the bilayers at $T = 298$ K. With smaller areas, the lipids at $T = 298$ K will have stronger interactions with neighboring sterol molecules than the lipids at $T = 325$ K, and this results in the larger condensing and chain ordering effects seen for the bilayers at $T = 298$ K. In comparing the data in Figure 6 for different ethanol concentrations, we see that carbon atoms 2−4 (see atom C3 in Figure 1) consistently show less ordering upon addition of ergosterol molecules than the ends of the acyl chains. Because the ergosterol hydroxyl group interacts favorably with the carbonyl oxygen atoms (Figure 3), the sterol rings should have a greater effect on chain order in the middle and the end of the chain than the top of the chain. We saw in Figure 2 that as the ethanol concentration increases, the ergosterol profiles broaden. This increased ergosterol density in the bilayer center results in the large X values seen for carbon 12−15 in a 15 vol % ethanol solution in Figure 6c.

For DMPC/cholesterol bilayers in the L_d phase and in the presence of a 2.2 M ethanol solution, Barry et al. found that ethanol molecules cause a greater decrease in the average order

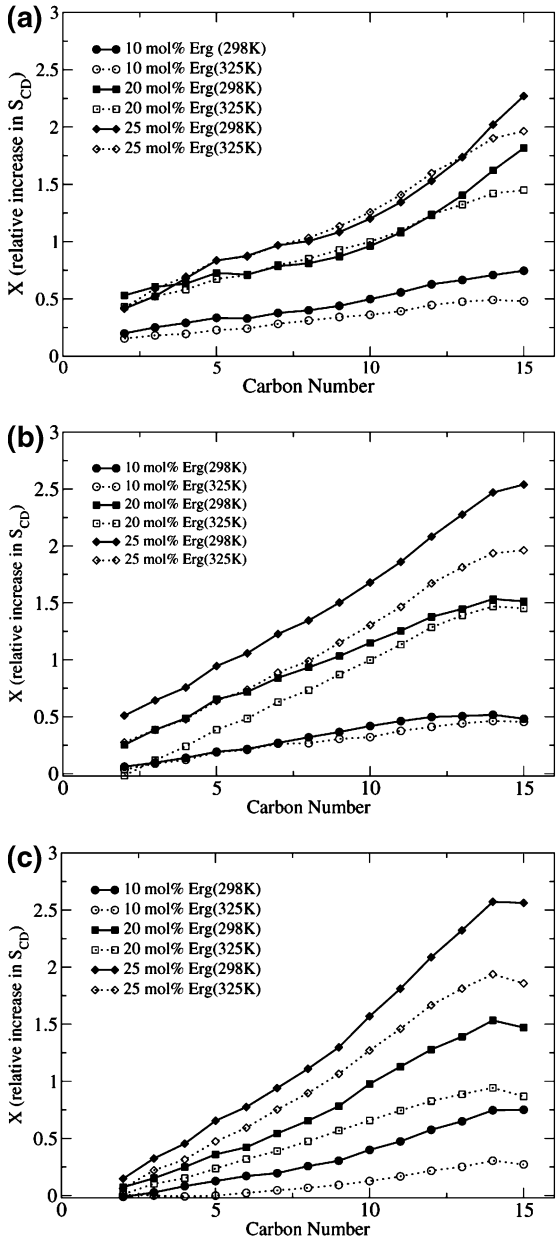

Figure 6. Relative increase in *sn*-2 S_{CD} resulting from inclusion of ergosterol at (a) 0 vol %, (b) 10 vol %, and (c) 15 vol % ethanol.

parameter for bilayers containing 12.5 mol % cholesterol than for bilayers containing 25 mol % cholesterol. To determine if a similar trend is seen in our simulations, we calculated the change in average order parameter for each ethanol concentration, where X is modified as

$$X^{\mathrm{eth}} = \frac{S_{\mathrm{CD}}^{\mathrm{eth}} - S_{\mathrm{CD}}}{S_{\mathrm{CD}}} \tag{5}$$

with $S_{\mathrm{CD}}^{\mathrm{eth}}$ referring to ethanol containing systems. The results in Figure 7 show that systems with 25 mol % ergosterol are more ordered for 10 and 15 vol % ethanol solutions than bilayers that contain 10 and 20 mol % ergosterol, with an exception being seen in the 10 mol % ergosterol system at $T = 325$ K. It is also interesting that the 0 mol % ergosterol systems have such large X^{eth} values. Because the X^{eth} values are averaged over all acyl chain atoms, it is not apparent from this number which

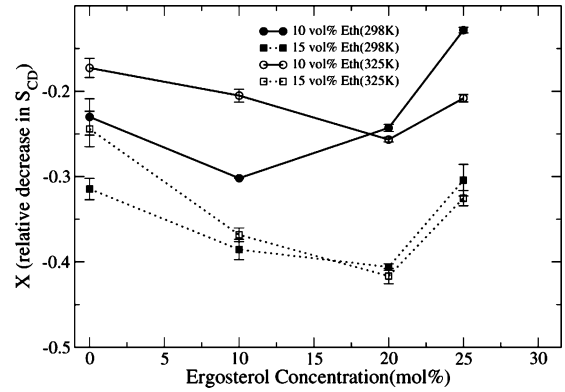

Figure 7. Relative decrease in *sn*-2 S_{CD} for 0, 10, and 15 vol % ethanol.

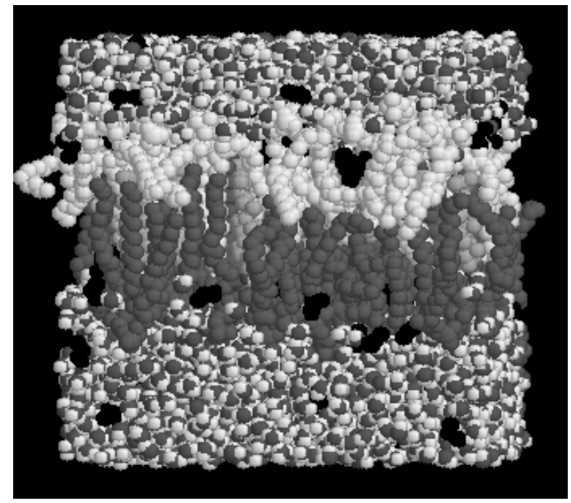

Figure 8. Picture of system 20−15 at $T = 298$ K. Interdigitation can be seen between the top leaflet lipids (white) and the bottom leaflet lipids (dark gray). Ergosterol molecules are light gray and ethanol molecules are black.

chain regions are the most disordered by the inclusion of ethanol. As seen in Figure 5, the 0 mol % ergosterol system at $T = 298$ K has the smallest order parameter values, especially for the atoms located in the middle (C6−C12) of the acyl chains. However, for the 10, 20, and 25 mol % ergosterol systems, the ergosterol molecules help order this region and hence the ethanol molecules have a larger disordering effect near the carbonyl groups than they did for the 0 mol % system.

Leaflet Interdigitation. One possible cause of stuck fermentations is an ethanol-induced change in yeast lipid membrane structures, which leads to deleterious changes in the conformations of important transmembrane proteins.[3,4]

Interdigitation occurs when lipid chains from one bilayer leaflet are found in a region of space normally only occupied by lipid chains from the opposite leaflet (example in Figure 8). One effect of interdigitation is a decrease in bilayer thickness. Interdigitation has been studied both by experiment[8,10−12,46,47] and via theory and simulations.[48−50] Figure 9 shows that at $T =$ 298 K, the distance between the density peaks for the lipid chains in the 15 vol % ethanol system is smaller than the 0 vol %. This indicates that the likelihood of finding interdigitation in the 15 vol % system is greater than the 0 vol % system and the squares and circles in Figure 9 represent interdigitated regions in the 15 vol % system that are not present in the 0 vol % system. To quantify the level of interdigitation in each system, we calculate the area under the density profile curves that exist

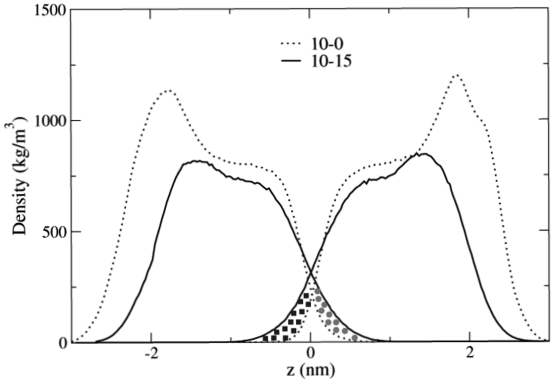

Figure 9. Density profiles for $10-0_{298}$ and $10-15_{298}$. The squares and circles show interdigitated regions that exist in the 15 vol % system and not in the 0 vol % system. The black squares represent lipid density from the top leaflet (0−3 nm) found in the bottom leaflet and the gray circles represent lipid density from the bottom leaflet found in the top leaflet.

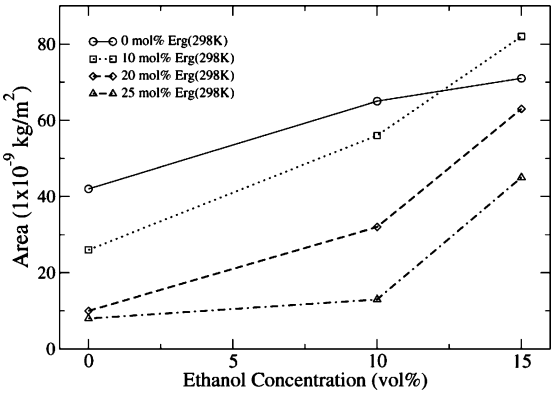

Figure 10. Interdigitated area (10^{-9} kg/m^2) from the density profile curves at $T = 298$ K. The likelihood of finding the interdigitated phase in a system increases with area.

in the opposing leaflet. Therefore, one integration limit is $z = 0$, which represents the bilayer center, and the second limit is where the density profile curve is equal to 0. Figure 10 shows that the 25 mol % ergosterol system has a similar amount of interdigitation for both the 0 and 10 vol % ethanol solutions. This is in contrast to the 0, 10, and 20 mol % ergosterol systems that show an increase in interdigitation when the ethanol concentration is increased from 0 to 10 vol %. However, in a 15 vol % ethanol concentration, the amount of interdigitation in all systems increases significantly. Using MPA experiments, Tierney et al. constructed a phase diagram for the DPPC/ergosterol/ethanol system at $T = 297$ K and we use their diagram to estimate how the quantities in Figure 10 correlate with specific lipid phases. According to the phase diagram, system $10-15_{298}$ (area: 82.5 kg/nm^2) is in the interdigitated phase, systems $20-10_{298}$ and $25-10_{298}$ (areas: 13.5 - 31.7 kg/nm^2) coexist in the L_o and the S_o phases, and the remaining systems are "gel-like" (areas: 44.8−63.1 kg/nm^2).[12] Hence, of the systems that we examined, only system $10-15_{298}$ fits into the interdigitated category and this result is similar to what was seen in a fluorescence spectroscopy experiment, where Komatsu et al. found that 20 mol % cholesterol inhibits the formation of the ethanol-induced interdigitated phase.[47]

Because the MPA vesicles included at least 10 mol % ergosterol, we compare the interdigitation in the $0-10_{298}$ system (no ergosterol) with density meter measurement experiments, where it was found that a DPPC bilayer was in the interdigitated state for an ethanol concentration of 76 mg/mL ethanol

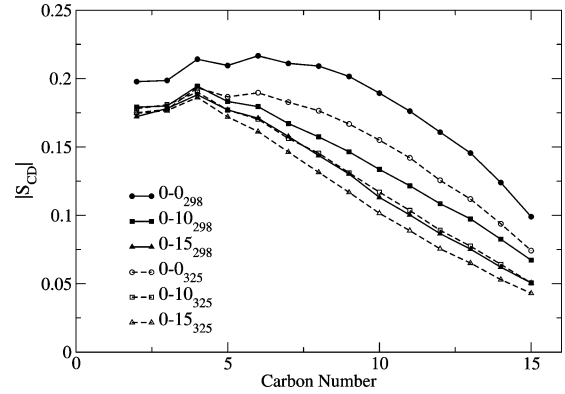

Figure 11. DPPC *sn*-2 acyl chain order parameters for $T = 298$ K and $T = 325$ K.

TABLE 4: Ethanol Crossings for $T = 298$ K and $T = 325$ K

ethanol crossing/ 10 ns	0−10	0−15	10−10	10−15	20−10	20−15	25−10	25−15
$T = 298$ K	0	3	2	4	0	2	0	3
$T = 325$ K	3	8	4	13	0	5	0	3

(equivalent to the 10 vol %) at $T = 298$ K.[8] The area for $0-10_{298}$ is 65 kg/nm^2 (Figure 10), which, on the basis of the calibrated area/phases seen above, places it between the "gel-like" and interdigitated phases.

The interactions between the DPPC lipids, ergosterol molecules and ethanol molecules that result in the trends seen in Figure 10 are quite complex. As was shown in Tables 1−3, bilayer thinning increases with an increase in ethanol concentration. However, because interdigitation reduces the conformational freedom of the acyl chain ends, one might also expect a reduction in the disordering effect of ethanol with an increase in ethanol concentration. Figure 11 shows that this is indeed the case, where the chain order decrease between system 0−0 and 0−10 is more than twice that seen between system 0−10 and 0−15 for both $T = 298$ K and $T = 325$ K.

Ethanol Crossings. The ability of alcohol molecules to permeate single-lipid bilayers has previously been studied via experiment and MD simulations and the permeability of ethanol molecules in a lipid/sterol bilayer has been examined using titration calorimetry.[51−54] The number of ethanol molecules that cross the bilayer during the 10 ns trajectory is shown in Table 4. An ethanol molecule is considered to have traversed the bilayer if it moves from the bottom leaflet into the top leaflet, or vice versa, by crossing through the center of the bilayer, which has the smallest bilayer lipid density. Therefore, we do not consider an ethanol molecule that moves to the opposite leaflet via the water phase as having crossed the bilayer. Also, a molecule that passes through the bilayer center and moves less than 0.25 nm into the new leaflet before returning to the original leaflet is not included in the crossing count.

Interestingly, the number of crossings is so small for the 8 systems at $T = 298$ K that it is not possible to determine the influence that ergosterol concentration has on membrane permeability. For the systems at $T = 325$ K, however, the membrane is the most permeable for an ergosterol concentration of 10 mol % and an ethanol concentration of 15 vol %.

Preferred Ethanol/Ergosterol Distance. To examine why the 10 mol % ergosterol concentration was more permeable to ethanol molecules than a 0, 20 or 25 mol % ergosterol concentration at $T = 325$ K, we determine if there is a region within the bilayer that is particularly amenable to ethanol

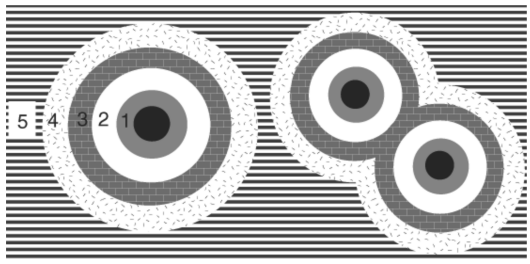

Figure 12. Ethanol molecules are assigned to bins 1−5 on the basis of the distance in *xy* between ethanol and ergosterol atoms. The black center represents an ergosterol molecule. Any partitioned ethanol molecule that has a distance <0.75 nm from an ergosterol atom is assigned to bin 1. If the distance between the partitioned ethanol molecule and the nearest ergosterol atom is greater than 0.75 nm, it is assigned to bin 2−5. Bin distance specifications: bin 1 (<0.75 nm), gray; bin 2 (0.75 ≤ 1.0), white; bin 3 (1.0 ≤ 1.25), brick patterned; bin 4 (1.25 ≤ 1.5), dots; bin 5 (1.5 <), horizontal lines. Note that because the lipid area is dependent on both temperature and ethanol/ergosterol concentration, the number of bins that exist vary by system.

insertion. To do this, we calculated the distance between the partitioned ethanol molecules and the ergosterol atoms. An ethanol molecule was considered to have partitioned into the bilayer if it was found between the P atom density profile peaks of the top and bottom leaflets. Next, each partitioned ethanol molecule was assigned to one of five bins on the basis of its distance from the closest ergosterol atom and the bin specifications are shown in Figure 12. To determine the appropriate bin for each partitioned ethanol molecule, we calculated the distance in *xy* between the ethanol oxygen atoms and all ergosterol atoms. Because the *z*-coordinates are not included in the calculation, the distances between the ethanol and ergosterol molecules are calculated separately for each leaflet. Additional details on this procedure can be found in the Methods.

Rather than look at the number of partitioned ethanol molecules per bin, a more interesting value is the number of partitioned ethanol molecules in each bin/bin area because this value would indicate if the ethanol molecules have an affinity for being located a specific distance from the ergosterol molecules. To determine this value, we calculated the bin area using a Monte Carlo-like method devised by Buffon in the 18th century.[55] A random number generator was used to produce 10 000 pairs of *x* and *y* coordinates and each of these points was assigned to bins 1−5 on the basis of the distance in *xy* between the point and the nearest ergosterol atom. The number of randomly generated points that was located in each bin was tabulated and the total number of points per bin was used to estimate the bin area. The bin areas for systems 10−0, 20−0, and 25−0 are shown in Figure 13 ($T = 298$ K) and Figure 14 ($T = 325$ K).

The results in Figures 15 and 16 show that for both $T = 298$ K and $T = 325$ K, bin 2 always has the highest ethanol/area ratio.

The lipids found in bin 1 (<0.75 nm) serve as annular lipids and solvate the ergosterol molecules. Using energy minimization, Vanderkooi found that DPMC−cholesterol interactions are stronger than either DMPC−DMPC or cholesterol−cholesterol interactions, with the largest energy contribution coming from nonbonded interactions between the α-surface of cholesterol and the acyl chains of DMPC.[56] Hence, with the existence of such favorable lipid/ergosterol interactions in bin 1, it may be hard for the ethanol molecules to partition into this region. Bin 2 may therefore serve as a transition zone, where it will contain lipids that are influenced by the lipid/ergosterol interactions in

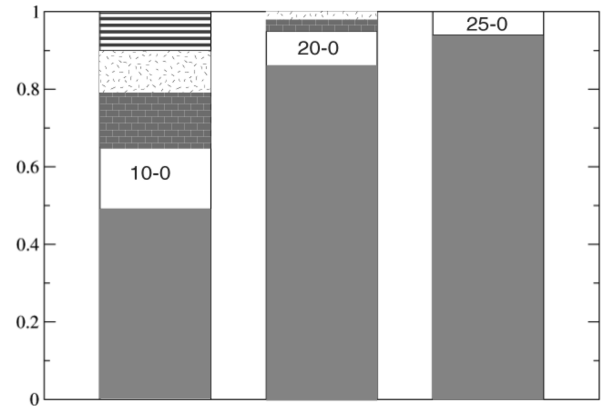

Figure 13. Fraction of the total area occupied by each bin at $T = 298$ K for systems 10−0, 20−0, and 25−0. Bin specifications and corresponding colors are described in Figure 12.

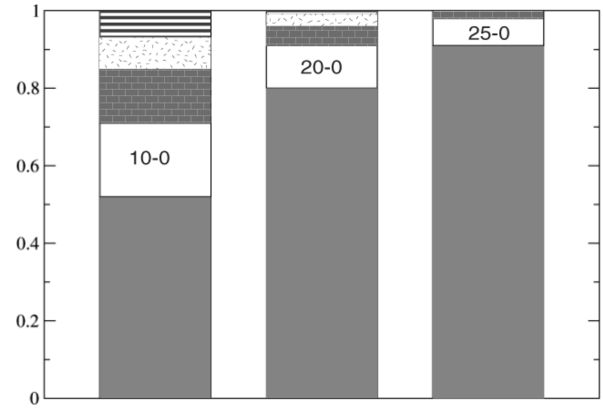

Figure 14. Fraction of the total area occupied by each bin at $T = 325$ K.

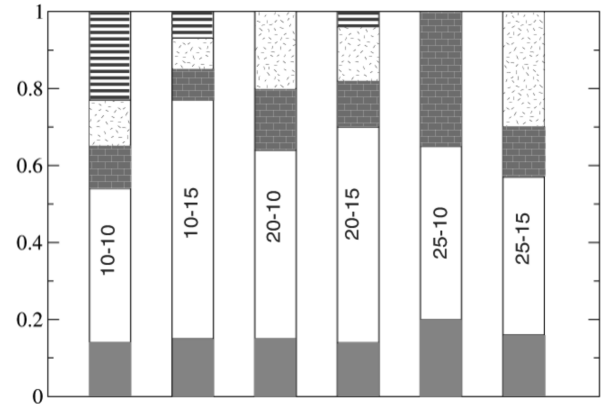

Figure 15. Fraction of partitioned ethanol molecules in each bin/bin area ($T = 298$ K).

neighboring bin 1. Because of this indirect influence of ergosterol, the lipids in bin 2 may not have the usual lipid/lipid interactions that are typically seen in single-component lipid bilayers and are more likely to be present in bins 3−5.

Discussion

In this study, we have examined how ergosterol molecules mitigate the fluidizing effects of ethanol molecules on lipid bilayers. Because stuck fermentations can be seen at ∼12−16 vol % ethanol, we are interested in examining how model yeast membranes are affected by the presence of such concentrated solutions. We found that, except for the systems, which contain

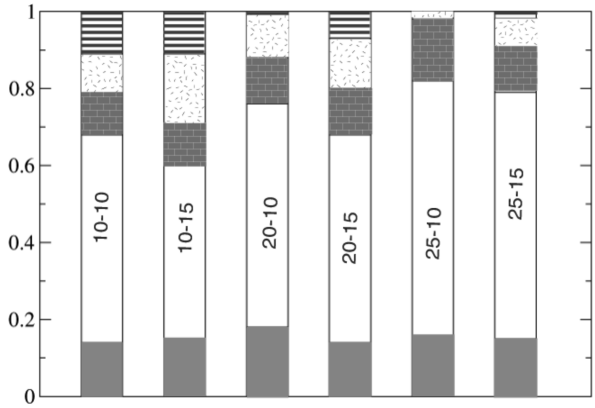

Figure 16. Fraction of partitioned ethanol molecules found in each bin/bin area ($T = 325$ K).

25 mol % ergosterol, the bilayers at $T = 325$ K were more permeable to ethanol molecules than the bilayers at $T = 298$ K. In a titration calorimetry experiment, Trandum et al. examined the ethanol partition coefficient in conjunction with unilamellar DMPC liposomes that contained various concentrations of cholesterol (0−40 mol %) over a range of temperatures (281−318 K).[57] They found an increased ethanol partitioning when the DMPC membrane contained low concentrations of cholesterol (< 10 mol %) and the system temperature was close to the lipid T_m.[57] An experimental DPPC/ergosterol phase diagram indicates that the systems at $T = 325$ K that have 10 mol % ergosterol will be in the L_d phase and phases that have 20 and 25 mol % ergosterol will be partly composed of the ordered L_o phase.[17] The lack of the L_o phase in the 10 mol % ergosterol system may make it easier for an ethanol molecule to permeate the bilayer. However, this does not explain why more ethanol molecules cross the bilayer in the 10 mol % than in the 0 mol % system. We found that for both $T = 298$ K and $T = 325$ K, the ethanol molecules prefer to be located ~0.75−1.0 nm from the nearest ergosterol atom. This may serve as a transition region and contain lipids that neither interact directly with the ergosterol molecules nor have bulk lipid properties. This lack of regular interlipid spacing may therefore present the ethanol molecules with an insertion location of minimal resistance and a non-ergosterol containing bilayer would not have this permeable transition region.

The relative increase in chain order that is seen for the 20 and 25 mol % ergosterol systems is similar at 298 and 325 K when no ethanol molecules are present. However, when a 15 vol % ethanol solution is added, the 25 mol % ergosterol solution at $T = 298$ K has the largest relative order, especially near the ends of the acyl chains. As the ethanol concentration increases, there is an increase in competition between the ethanol and ergosterol molecules to hydrogen bond with the DPPC carbonyl oxygen atoms. In response to this ethanol-induced crowding, the ergosterol molecules shift toward the bilayer center, resulting in an increase in ergosterol density in this region. The amount of interdigitation seen for the 25 mol % bilayer at $T = 298$ K is very similar in the presence of both 0 and 10 vol % ethanol solutions, indicating that the ergosterol molecules in this system are able to effectively counteract the ethanol molecules. However, at a 15 vol % ethanol solution, the amount of interdigitation more than triples and this ethanol concentration coincides with the concentrations seen in stuck fermentations. For the other three ergosterol concentrations (0, 10, 20 mol %), interdigitation is greater in the 10 vol % ethanol solution than the 0 vol % ethanol solution. This shows that the 25 mol % ergosterol system, which is similar to the ergosterol concentrations seen in yeast membranes, is unique in its ability to delay the onset of significant amounts of interdigitation.

Acknowledgment. This work was was supported by the NIH training grant in biomolecular technology (Grant T32-GM08799) and the U.S. Department of Agriculture (Grant 2007-02140). We gratefully acknowledge computer time at the Texas Advanced Computer Center (Grant TG-MCB070076N).

Note Added after Print Publication. This paper was published on the Web on February 4, 2009, and in the February 26, 2009, issue. An author name was misspelled. The electronic version was corrected and reposted to the Web issue on April 16, 2009. An Addition and Correction appears in the April 23, 2009, issue (Vol. 113, No. 16).

References and Notes

(1) Rass-Hansen, J.; Falsig, H.; Jorgensen, B.; Christensen, C. H. *J. Chem. Technol. Biotechnol.* **2007**, *82*, 329–333.
(2) Sanderson, K. *Nature* **2006**, *444*, 673–676.
(3) Block, D. E.; Bisson, L. F. Ethanol tolerance in Saccharomyces. In *Biodiversity and Biotechnology of Wine Yeasts*; Ciani, M. Ed.; Research Signpost: Kerala, India, 2002.
(4) Bisson, L. F. *Am. J. Enol. Vitic.* **1999**, *50*, 107–119.
(5) Bloom, M.; Mouritsen, O. G. *Can. J. Chem.* **1988**, *66*, 706–712.
(6) Thomas, D. S.; Hossack, J. A.; Rose, A. H. *Arch. Microbiol.* **1978**, *117*, 239–245.
(7) Chi, Z.; Arneborg, N. J. *Ind. Microb. Biotechnol.* **2000**, *24*, 75–78.
(8) Ohki, K.; Tamura, K.; Hatta, I. *J. Ind. Microb. Biotechnol.* **2000**, *24*, 75–78.
(9) Mou, J.; Yang, J.; Huang, C.; Shao, Z. *Biochemistry* **1994**, *33*, 9981–9985.
(10) Nambi, P.; Rowe, E. S.; McIntosh, T. J. *Biochemistry* **1988**, *27*, 9175–9182.
(11) Rowe, E. S. *Biochemistry* **1983**, *22*, 3299–3305.
(12) Tierney, K. J.; Block, D. E.; Longo, M. L. *Biophys. J.* **2005**, *89*, 2481–2493.
(13) Urbina, J. A.; Pekerar, S.; Le, H. B.; Patterson, J.; Montez, B.; Oldfield, E. *Biochim. Biophys. Acta* **1995**, *1238*, 163–176.
(14) Arneborg, N.; Hoy, C. E.; Jorgensen, O. B. *Yeast* **1995**, *11*, 953–959.
(15) Cramer, A. C.; Vlassides, S.; Block, D. E. *Biotechnol. Bioeng.* **2002**, *77*, 49–60.
(16) Vist, M. R.; Davis, J. H. *Biochemistry* **1990**, *29*, 451–464.
(17) Hsueh, Y.; Gilbert, K.; Trandum, C.; Zuckermann, M.; Thewalt, J. *Biophys. J.* **2005**, *88*, 1799–1808.
(18) Hsueh, Y.; Chen, M.; Patty, P. J.; Code, C.; Cheng, J.; Frisken, B. J.; Zuckermann, M.; Thewalt, J. *Biophys. J.* **2007**, *92*, 1606–1615.
(19) Barry, J. A.; Gawrisch, K. *Biochemistry* **1995**, *34*, 8852–8860.
(20) DeYoung, L. R.; Dill, K. A. *Biochemistry* **1988**, *27*, 5281–5289.
(21) Kleywegt, G. J.; Jones, T. A. *Acta Crystallogr.* **1998**, *D54*, 1119–1131.
(22) Hoeltje, M.; Foerster, T.; Brandt, B.; Engels, T.; von Rybinski, W.; Hoeltje, H. D. *Biochim. Biophys. Acta* **2001**, *1511*, 156–167.
(23) Tieleman, D. P.; Berendsen, H. J. C. *J. Chem. Phys.* **1996**, *105*, 4871–4880.
(24) Berger, O.; Edholm, O.; Jahnig, F. *Biophys. J.* **1997**, *72*, 2002–2013.
(25) van Gunsteren, W. F.; Kruger, P.; Billeter, S. R.; Mark, A. E.; Eising, A. A.; Scott, W. R. P.; Hunenberger, P. H.; Tironi, I. G. *Biomolecular Simulation: The GROMOS 96 Manual and User Guide*; Biomos Hochschulverlag AG an der ETH Zurich: Groningen, Netherlands, 1996.
(26) Berendsen, H. J. C.; Postma, J. P. M.; van Gunsteren, W. F.; Hermans, J. *Interaction models for water in relation to protein hydration*; Pullman, B. E., Ed.; Reidel: Dordrecht, The Netherlands, 1981.
(27) Lindahl, E.; Hess, B.; van der Spoel, D. *J. Mol. Mod.* **2001**, *7*, 306–317.
(28) Berendsen, H. J. C.; van der Spoel, D.; van Drunen, R. *Comput. Phys. Commun.* **1995**, *91*, 43–56.
(29) van der Spoel, D.; Lindahl, E.; Hess, B.; Groenhof, G.; Mark, A. E.; Berendsen, H. J. C. *J. Comput. Chem.* **2005**, *26*, 1701–1718.
(30) Berendsen, H. J. C.; Postma, J. P. M.; van Gunsteren, W. F.; DiNola, A.; Haak, J. R. *J. Chem. Phys.* **1984**, *81*, 3684–3690.
(31) Hess, B.; Bekker, H.; Berendsen, H. J. C.; Fraaije, J. G. E. M. *J. Comput. Chem.* **1997**, *18*, 1463–1472.
(32) Essman, U.; Perela, L.; Berkowitz, M. L.; Darden, H. L. T.; Pedersen, L. G. *J. Chem. Phys.* **1995**, *103*, 8577–8592.

(33) Hofs, C.; Lindahl, E.; Edholm, O. *Biophys. J.* **2003**, *84*, 2192–2206.
(34) Jönsson, P. *Acta Crystallogr.* **1976**, *B32*, 232–235.
(35) Leekumjorn, S.; Sum, A. K. *Biochim. Biophys. Acta* **2007**, *1768*, 354–365.
(36) Wiener, M. C.; Suter, R.; Nagle, J. F. *Biophys. J.* **1989**, *55*, 315–325.
(37) Nagle, J.; Zhang, R.; Tristram-Nagle, S.; Sun, W.; Petrache, H.; Suter, R. *Biophys. J.* **1996**, *70*, 1419–1431.
(38) Cournia, Z.; Ullmann, G. M.; Smith, J. C. *J. Phys. Chem. B* **2007**, *111*, 1786–1801.
(39) Shieh, H.-S.; Hoard, L. G.; Nordman, C. E. *Acta Crystallogr.* **1981**, *B37*, 1538–1543.
(40) Chiu, S. W.; Jakobsson, E.; Mashl, R. J.; Scott, H. L. *Biophys. J.* **2002**, *83*, 1842–1853.
(41) McIntosh, T. J. *Biochim. Biophys. Acta* **1978**, *513*, 43–58.
(42) Yeagle, P. Y.; Martin, R. B. *Biochem. Biophys. Res. Commun.* **1976**, *69*, 775–780.
(43) Henriksen, J.; Rowat, A. C.; Brief, E.; Hsueh, Y. W.; Thewalt, J. L.; Zuckermann, M. J.; Ipsen, J. H. *Biophys. J.* **2006**, *90*, 1639–1649.
(44) Feller, S. E.; Brown, C. A.; Nizza, D. T.; Gawrisch, K. *Biophys. J.* **2002**, *82*, 1396–1404.
(45) Patra, M.; Salonen, E.; Terama, E.; Vattulainen, I.; Faller, R.; Lee, B. W.; Holopainen, J.; Karttunen, M. *Biophys. J.* **2006**, *90*, 1121–1135.
(46) Rowe, E. S.; Cutrera, T. A. *Biochemistry* **1990**, *29*, 10298–10404.
(47) Komatsu, H.; Rowe, E. S. *Biochemistry* **1991**, *30*, 2463–2470.
(48) Kranenburg, M.; Vlaar, M.; Smit, B. *Biophys. J.* **2004**, *87*, 1596–1605.
(49) Kranenburg, M.; Smit, B. *FEBS* **2004**, *568*, 15–18.
(50) Frischknecht, A. L.; Frink, L. J. D. *Biophys. J.* **2006**, *91*, 4081–4090.
(51) Ly, H. V.; Longo, M. L. *Biophys. J.* **2004**, *87*, 1013–1033.
(52) Patra, M.; Karttunen, M.; Hyvonen, M.; Falck, E.; Vattulainen, I. *Biophys. J.* **2004**, *84*, 3636–3645.
(53) Dickey, A. N.; Faller, R. *Biophys. J.* **2007**, *92*, 2366–2376.
(54) Rowe, E. S.; Zhang, F.; Leung, T. W.; Parr, J. S.; Guy, P. T. *Biochemistry* **1998**, *37*, 2430–2440.
(55) Buffon, G. *Histoire naturelle, generale er particuliere, Supplément 4. Essai d'arithmetique morale*; McGraw-Hill Book Co., Inc.: New York, 1777.
(56) Vanderkooi, G. *Biophys. J.* **1994**, *66*, 1457–1468.
(57) Trandum, C.; Westh, P.; Jorgensen, K.; Mouritsen, O. G. *Biophys. J.* **2000**, *78*, 2486–2492.

JP803092Z